GEOPHYSICAL RESEARCH LETTERS, VOL. 37, L14502, doi:10.1029/2010GL043853, 2010

Spatial patterns of basal drag inferred using control methods from a full-Stokes and simpler models for Pine Island Glacier, West Antarctica

M. Morlighem,[1,2] E. Rignot,[1,3] H. Seroussi,[1,2] E. Larour,[1] H. Ben Dhia,[2] and D. Aubry[2]

Received 4 May 2010; revised 4 June 2010; accepted 22 June 2010; published 30 July 2010.

[1] Basal drag is a fundamental control on ice stream dynamics that remains poorly understood or constrained by observations. Here, we apply control methods on ice surface velocities of Pine Island Glacier, West Antarctica to infer the spatial pattern of basal drag using a full-Stokes (FS) model of ice flow and compare the results obtained with two commonly-used simplified solutions: the MacAyeal shelfy stream model and the Blatter-Pattyn model. Over most of the model domain, the three models yield similar patterns of basal drag, yet near the glacier grounding-line, the simplified models yield high basal drag while FS yields almost no basal drag. The simplified models overestimate basal drag because they neglect bridging effects in an ice stream region of rapidly varying ice thickness. This result reinforces theoretical studies that a FS treatment of ice flow is essential near glacier grounding lines. **Citation:** Morlighem, M., E. Rignot, H. Seroussi, E. Larour, H. Ben Dhia, and D. Aubry (2010), Spatial patterns of basal drag inferred using control methods from a full-Stokes and simpler models for Pine Island Glacier, West Antarctica, *Geophys. Res. Lett.*, *37*, L14502, doi:10.1029/2010GL043853.

1. Introduction

[2] Pine Island Glacier, in West Antarctica, has the largest ice discharge of all West Antarctic ice streams. It has been retreating, thinning and accelerating steadily since at least the 1970s [*Rignot*, 2008]. The glacier acceleration at present is several times larger than that estimated for the 1970-1980 and is increasing every year [*Rignot*, 2008].

[3] The changes taking place on Pine Island Glacier cannot be explained using simple ice flow models such as the Shallow Ice Approximation (SIA) [*Hutter*, 1983] where stresses are determined locally and all components other than vertical shear are neglected. This limitation has raised the issue of the degree of sophistication needed from numerical models to replicate the observed ice dynamics. The full-Stokes equations make no approximation in the stress tensor and therefore allow better modeling of flow dynamics, but they typically require two orders of magnitude more computational resources than simpler two-dimensional (2D) models. A full-Stokes solution may not be needed everywhere, depending on the ice stream stress regime, if higher order terms are negligible.

[4] Here, we address the issue of comparing different flow models using data assimilation techniques to infer the pattern of basal drag of Pine Island Glacier. Basal drag is a fundamental control on ice flow, yet it is poorly understood, as it is difficult to observe directly. We infer basal drag from satellite observations of surface motion derived from interferometric synthetic-aperture radar (InSAR) data using a data assimilation technique. The control methods, initially introduced to glaciology by *MacAyeal* [1993] for 2D flow modeling are generalized to full 3D velocity fields. The results obtained from the full-Stokes model are compared with results obtained using two simpler, more practical models: 1) the MacAyeal's shelfy-stream model or Shallow Shelf Approximation model (SSA) [*MacAyeal*, 1989], and 2) the Blatter-Pattyn's higher-order model (BP) [*Pattyn*, 2003]. We conclude by making recommendations on the degree of sophistication of the solution needed to model ice stream flow.

2. Methods

2.1. Ice Flow Models

[5] The most complete ice flow model is the full-Stokes set of equations (FS), which includes the momentum balance and the incompressibility equations. The acceleration being negligible, these equations are, respectively:

$$\nabla \cdot \sigma + \rho\, \mathbf{g} = \mathbf{0} \tag{1}$$

$$\mathrm{Tr}(\dot{\varepsilon}) = 0 \tag{2}$$

where $\nabla \cdot \sigma$ is the divergence vector of the stress tensor, σ, $\mathrm{Tr}(\dot{\varepsilon})$ is the trace of the strain rate tensor, $\dot{\varepsilon}$, ρ is the ice density and $\mathbf{g}$ the acceleration due to gravity. Ice is treated as an isotropic and incompressible material. The pressure, P, is introduced as a Lagrange multiplier to insure the incompressibility/continuity equation (2). The behavior law of ice is:

$$\sigma' = 2\mu\dot{\varepsilon} \tag{3}$$

where $\sigma' = \sigma + P\mathbf{I}$ is the deviatoric stress tensor, $\mathbf{I}$ is the identity matrix and μ is the non-linear viscosity, which follows a Norton-Hoff law [*Glen*, 1955].

$$\mu = B\sigma_e^{\frac{1-n}{n}} \tag{4}$$

B is the ice hardness, n the Glen's law coefficient (here chosen as $n = 3$ [*Paterson*, 1994]) and σ_e the effective stress.

[1]Jet Propulsion Laboratory, California Institute of Technology, Pasadena, California, USA.
[2]Laboratoire MSSMat, UMR 8579, École Centrale Paris, CNRS, Châtenay-Malabry, France.
[3]Department of Earth System Science, University of California, Irvine, California, USA.

0094-8276/10/2010GL043853

Equation (1) may be written in terms of strain rate tensor as follows:

$$\nabla \cdot (2\mu\dot{\varepsilon}) - \nabla P + \rho\, \mathbf{g} = \mathbf{0} \tag{5}$$

Mini-elements [*Gresho and Sani*, 2000b] are used in the finite element implementation of this model to fulfill the compatibility Ladyzhenskaya-Babuška-Brezzi (LBB) condition.

[6] A simplified three-dimensional (3D) model from *Blatter* [1995] and *Pattyn* [2003] (BP) is derived from FS by making two assumptions: 1) the horizontal gradients of vertical velocities are negligible compared to the vertical gradients of horizontal velocities:

$$\dot{\varepsilon}_{xz} = \frac{1}{2}\frac{\partial u}{\partial z}; \qquad \dot{\varepsilon}_{yz} = \frac{1}{2}\frac{\partial v}{\partial z} \tag{6}$$

and 2) the bridging effects [*van der Veen and Whillans*, 1989] are negligible, which reduces the third equation of the momentum balance (equation (5)) to:

$$\frac{\partial}{\partial z}\left(2\mu\frac{\partial w}{\partial z}\right) - \frac{\partial P}{\partial z} - \rho g = 0 \tag{7}$$

where (u,v,w) are the x, y and z components of the velocity vector $\mathbf{v}$, x and y are horizontal and z is the vertical axis.

[7] Finally, the third model, or SSA [*MacAyeal*, 1989], assumes in addition that the vertical shear is negligible:

$$\dot{\varepsilon}_{xz} = 0; \qquad \dot{\varepsilon}_{yz} = 0 \tag{8}$$

This assumption reduces the equations to a 2D model, as u and v do not depend on depth z. The vertical velocity, w, is deduced from the horizontal velocities, u and v, using equation (2) in BP and SSA.

2.2. Thermal Model

[8] Ice hardness, B, is mainly temperature dependent, so we need a thermodynamic model of the ice sheet to calculate its value. The thermal equation is derived from the energy conservation equation and includes conduction and advection in all three directions. We assume that the ice sheet is in thermal steady state, which leads to:

$$\frac{\partial T}{\partial t} = 0; \qquad \mathbf{v} \cdot \nabla T = \frac{k_{th}}{\rho c}\Delta T + \Phi \tag{9}$$

T is the ice temperature, t is time, k_{th} is the ice thermal conductivity, c the ice heat capacity, Φ is the deformational heating and Δ is the Laplace operator. This equation is solved using the Streamline Upwind Petrov-Galerkin (SUPG) [*Gresho and Sani*, 2000a]) formulation of the finite element method to prevent potential numerical oscillations due to dominant advection terms. The temperature T is forced to remain below the pressure melting point using an iterative penalty-based scheme as in a contact problem [*Courant*, 1943].

2.3. Boundary Conditions

[9] The upper boundary condition of the ice flow model is a stress-free surface. A friction law is applied at the ice-bedrock interface. The basal drag is modeled following *Paterson* [1994] written in a Coulomb-like law of friction:

$$\tau_{\mathbf{b}} = -k^2 N \mathbf{v}_{\mathbf{b}} \tag{10}$$

where $\mathbf{v_b}$ is the basal velocity vector tangential to the glacier base plane, N is the effective pressure on the glacier base, here equal to $N = \rho g h$, where h is the height of the ice sheet surface above buoyancy, $\tau_{\mathbf{b}}$ is the tangential component of the external force, $\sigma \cdot \mathbf{n}$, $\mathbf{n}$ is the outward pointing normal vector and k^2 is a positive constant (i.e., stress opposes the motion). Since we are only using a static model of Pine Island Glacier, the choice of fiction law is not critical: the data assimilation procedure converges toward the same value of $\tau_{\mathbf{b}}$ regardless of the form of equation (10). Water pressure is imposed on the ice-sea water interface. The observed surface velocity is imposed on the remaining boundaries.

[10] In the thermal model, the surface temperature is the mean annual air temperature from *Giovinetto et al.* [1990]. On grounded ice, we imposed a geothermal heat flux [*Maule et al.*, 2005] and a frictional heat flux equal to $\tau_{\mathbf{b}} \cdot \mathbf{v_b}$. On the ice shelf, basal drag is zero, thermal modeling is unresolved due to the complexity of ice-ocean interaction and the ice hardness B is inferred using an independent control method. Surface topography is from a digital elevation model of Antarctica from *Bamber et al.* [2009], a firn depth correction from *van den Broeke* [2008] and ice thickness is from *Vaughan et al.* [2006].

2.4. Control Method

[11] The basal drag coefficient k in equation (10) cannot be measured directly and is inferred using a control method. We use a partial differential equations constrained optimization algorithm similar to *Vieli and Payne* [2003], which consists in a gradient minimization of a cost function that measures the misfit between observed (u_{obs}, v_{obs}) and modeled (u, v) horizontal surface velocities. The algorithm relies on the adjoint method, which calculates the gradient of the cost function with respect to the unknown parameters. This cost function is usually taken as:

$$J = \int\int_{\Omega} \frac{1}{2}(u - u_{obs})^2 + \frac{1}{2}(v - v_{obs})^2 d\Omega \tag{11}$$

This cost function works better in areas of high-velocity than in slow moving regions because the adjoint state (Lagrange multipliers vector) is larger where the velocity misfit $|u - u_{obs}|$ is high, which occurs in regions of high speed. To minimize this effect, we introduce a new cost function that measures the logarithm of the misfit:

$$J = \int\int_{\Omega} \overline{V}^2 \left(\log\left(\frac{\sqrt{u^2 + v^2} + \varepsilon}{\sqrt{{u_{obs}}^2 + {v_{obs}}^2} + \varepsilon}\right)\right)^2 d\Omega \tag{12}$$

where $\overline{V}$ is an averaged velocity magnitude used for dimensional purposes, ε is a minimum velocity used to avoid zero velocities, and log is the natural logarithm. This cost function enables a robust estimation of the basal drag coefficient after only a few iterations over the entire model domain. A Tikhonov regularization term, which penalizes the oscillations of the basal drag coefficient, k, is added to stabilize the inversion [*Vogel*, 2002].

[12] The finite element stiffness matrix is assumed to be independent of the velocity in order to have a self-adjoint

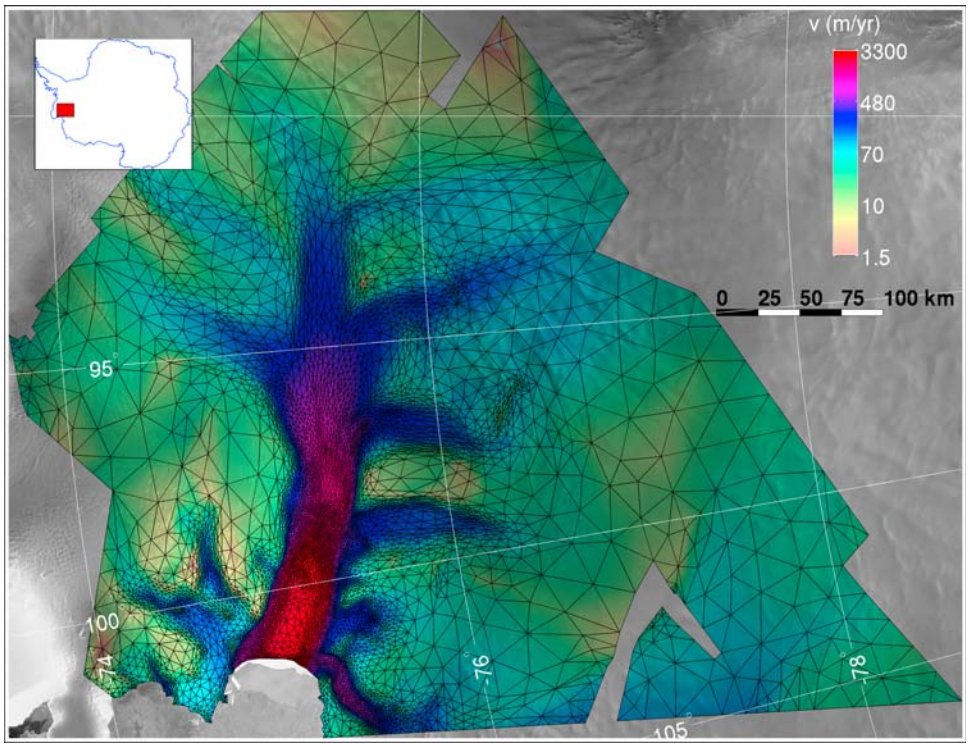

Figure 1. Pine Island Glacier surface velocity field in 1996 from *Rignot et al.* [2002] and 2D anisotropic mesh of 15,000 elements, which is vertically extruded to generate a 3D mesh.

problem. This assumption is not correct as the viscosity, μ, depends on the strain rate, but it allows an easier calculation of the adjoint state for the three ice flow models and is widely employed [*MacAyeal*, 1993].

[13] This data assimilation technique has successfully been extended to BP and FS. The major difference with SSA is that only the surface horizontal velocities are taken into account in the cost function evaluation, while its gradient with respect to k is computed at the base only.

[14] At each iteration of the optimization procedure, we recalculate a thermo-mechanical equilibrium solution and accordingly update the ice hardness B on grounded ice to ensure consistency between the ice flow and the viscosity μ.

2.5. Mesh

[15] To limit the number of elements while maximizing spatial resolution, we use an anisotropic mesh. It can be shown that an interpolation-based a-priori error estimate of a finite element $P1$ solution (piecewise linear) depends only on its Hessian [*Habashi et al.*, 2000], provided that the solution is regular enough.

[16] Here, we base our metric on the observed surface velocities Hessian matrix to equi-distribute the a-priori error estimate using an edge-based anisotropic mesh optimization methodology inspired by *Frey* [2001] and *Hecht* [2006]. The final 2D mesh is shown on Figure 1 and is vertically extruded to form a 3D adapted mesh of 103,000 elements with 8 vertical layers.

3. Results

[17] We run the same experiment for the three ice flow models using the same mesh and boundary conditions. The inferred patterns of basal drag and the velocity misfits are shown on Figure 2. The optimization scheme converges well for the three models and the modeled velocities reproduce the observed velocities with an excellent accuracy, even in slow-moving regions where InSAR observations are less accurate. The average misfits

$$\overline{M} = \int\int_S \left| \sqrt{u^2 + v^2} - \sqrt{u_{obs}^2 + v_{obs}^2} \right| dS \qquad (13)$$

for the entire domain are: $\overline{M}_{SSA}$ = 27 m/yr for SSA, $\overline{M}_{BP}$ = 11.1 m/yr for BP and $\overline{M}_{FS}$ = 10.4 m/yr for FS. The largest errors are found on fast flow areas. On the ice stream proper, we have $\overline{M}_{SSA}$ = 62 m/yr, which represents 5% of the average speed in this area, $\overline{M}_{BP}$ = 22.9 m/yr (1.8%) and $\overline{M}_{FS}$ = 19.5 m/yr (1.6%).

[18] The spatial patterns of basal drag inferred from the three models (Figure 2) are similar to those inferred from simpler models [*Joughin et al.*, 2009; *Vieli and Payne*, 2003]. The basal drag from FS is closer to BP, as expected since SSA is the most simplified solution. In most areas, the difference in basal drag between solutions is minimal and the agreement between observed and modeled velocity remains excellent. Near the grounding-line, however, SSA and BP exhibit a high basal drag (80 kPa), while the basal drag inferred from FS is less than 10 kPa (Figure 3).

4. Discussion

[19] The bed elevation of Pine Island Glacier rises steeply downstream toward the grounding-line: in 20 km the bed rises from -1200m to -550m, i.e., a slope of +3%. It is in

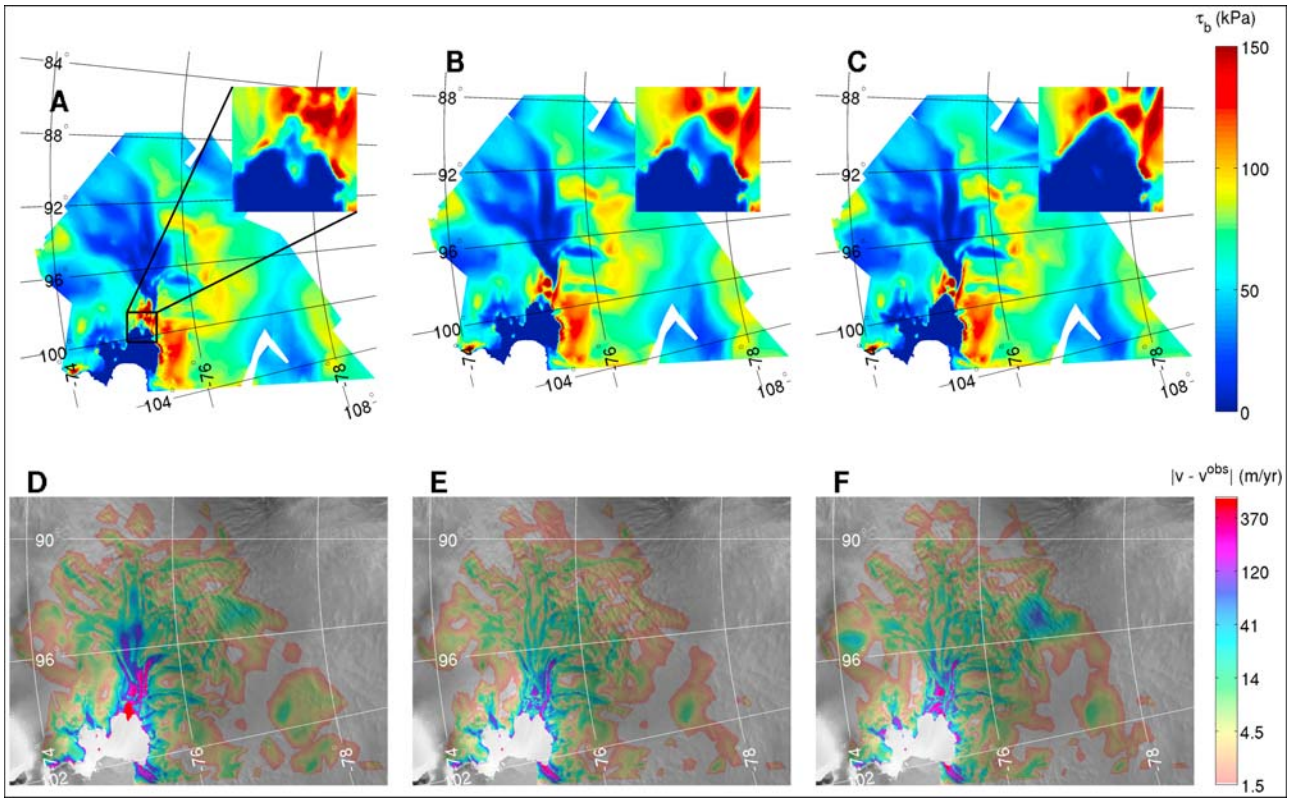

Figure 2. Magnitude of the basal drag, τ_b, in kPa, inferred from observations using (a) SSA, (b) BP, (c) FS, and velocity misfits between observed and modeled velocities in m/yr, using (d) SSA, (e) BP, and (f) FS.

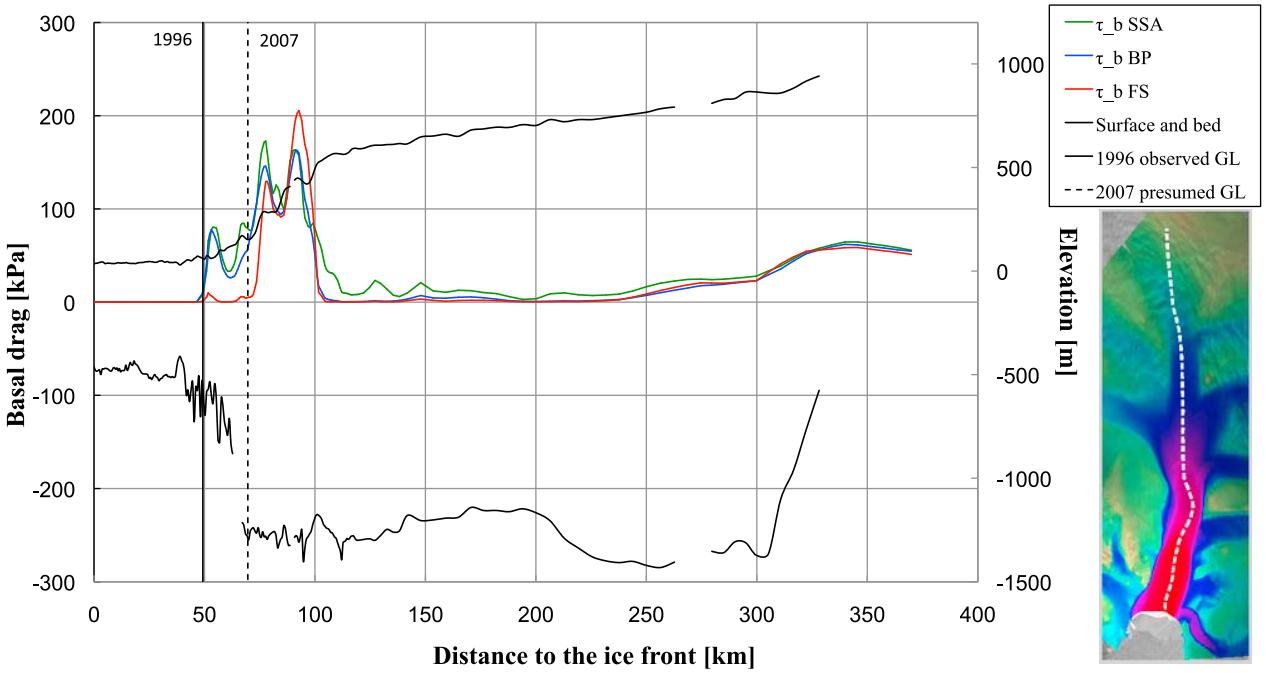

Figure 3. Comparison of inferred basal drag, τ_b, in kPa, SSA (green line), BP (blue line) and FS (red line) along a flowline. Bed and surface elevations are the black lines [*Thomas et al.*, 2004]. Vertical lines are the 1996 observed (black solid) and 2007 presumed (black dashed) grounding-line positions [*Rignot*, 2008].

this region that the difference in basal drag patterns between the three models is the largest.

[20] BP and SSA both neglect the bridging effect, which reduces the vertical equation of the momentum balance to equation (7). Applying the stress-free boundary condition on the upper surface gives:

$$\sigma_{zz} = \rho g (z - s) \tag{14}$$

At the base of the glacier, we therefore have $\sigma_{zz} = -\rho g H$, where H is the ice thickness. Although this approximation is generally true almost everywhere, our calculation of σ_{zz} at the base of the glacier using FS shows that σ_{zz} and $\rho g H$ differ by up to 2% in the grounding-line region. The vertical stress applied by the bedrock is indeed slightly larger than the ice column weight, $\rho g H$, as the rising bedrock pushes the ice upward. In FS, the rising bed is reducing the ice velocity without additional basal drag. In SSA and BP, the bridging stress is neglected, and the models can only fit the data by increasing basal drag. This increase is not physical but due to an incomplete physics in the two simplified models.

[21] Interestingly, the low basal drag inferred from FS corresponds to a region where the grounding-line probably retreated between 1996 and 2007 [*Rignot*, 2008]. In this area, the ice surface was only 15 to 40 meters above hydrostatic equilibrium in year 2002 [*Thomas et al.*, 2004]. Basal drag should not be high in this region since it is proportional to the overburden pressure, which is expected to be small. The FS solution is therefore more consistent with the ice physics near the grounding-line.

[22] To model dynamic glacier changes, e.g., grounding-line retreat, it would seem essential to employ a model that fully represents the ice flow dynamics. As we discussed above, SSA and BP are not adequate near the grounding-line because of simplified physics. If the FS solution is not used, the model would be initiated using values of basal drag that are too high and this would impact the simulation of grounding-line retreat.

[23] Using a FS solution near the grounding-line is also mandated by theoretical studies to be essential in dynamic models to analyze grounding-line stability [*Nowicki and Wingham*, 2008] and migration [*Durand et al.*, 2009].

[24] The conclusion of our experiment has a broader character than just the case of Pine Island Glacier. We would expect similar issues with other fast-moving glaciers with a steeply rising bed near the grounding-line and high stresses of all orders in that region. This clearly suggests that near the grounding-line of ice streams, treating ice flow with the complete physics of FS is essential.

5. Conclusions

[25] The three ice flow models employed in this study reproduce the observed velocities of Pine Island Glacier well and yield similar patterns of basal drag almost everywhere. This suggests that FS is not required everywhere to model ice sheet flow or ice shelf flow. In the grounding-line region, however, three-dimensional effects are pronounced and FS is essential to infer a correct pattern of basal drag and to capture all higher order stresses. The correct representation of all stresses is probably even more important to model grounding-line migration.

[26] Because FS is however computationally intensive, it is prohibitive for large-scale modeling. We therefore recommend hybrid models that use a simple two-dimensional model on ice shelves, a 3D BP on grounded ice but FS near the grounding-line.

[27] **Acknowledgments.** We would like to thank the two reviewers for their constructive comments. This work was performed at the Jet Propulsion Laboratory, California Institute of Technology, at the Department of Earth System Science, University of California Irvine, and at Laboratoire MSSMat, École Centrale Paris, under a contract with the National Aeronautics and Space Administration, Cryospheric Sciences Program.

References

Bamber, J. L., J. L. Gomez-Dans, and J. A. Griggs (2009), A new 1 km digital elevation model of the Antarctic derived from combined satellite radar and laser data—Part 1: Data and methods, *Cryosphere*, *3*(1), 101–111.

Blatter, H. (1995), Velocity and stress-fields in grounded glaciers: A simple algorithm for including deviatoric stress gradients, *J. Glaciol.*, *41*(138), 333–344.

Courant, R. (1943), Variational methods for the solution of problems of equilibrium and vibrations, *Bull. Am. Math. Soc.*, *49*, 1–23.

Durand, G., O. Gagliardini, T. Zwinger, E. Le Meur, and R. Hindmarsh (2009), Full Stokes modeling of marine ice sheets: Influence of the grid size, *Ann. Glaciol.*, *50*(52), 109–114.

Frey, P. J. (2001), Yams, a fully automatic adaptive isotropic surface remeshing procedure, *Tech. Rep. RT-0252*, Inst. Natl. de Rech. en Inf. et en Autom., Rocquencourt, France.

Giovinetto, M., N. Waters, and C. Bentley (1990), Dependence of Antarctic surface mass balance on temperature, elevation, and distance to open ocean, *J. Geophys. Res.*, *95*(D4), 3517–3531.

Glen, J. (1955), The creep of polycrystalline ice, *Proc. R. Soc. A*, *228* (1175), 519–538.

Gresho, P. M., and R. L. Sani (2000a), *Incompressible Flow and the Finite Element Method*, vol. 1, *Advection-Diffusion*, 472 pp., John Wiley, Hoboken, N. J.

Gresho, P. M., and R. L. Sani (2000b), *Incompressible Flow and the Finite Element Method*, vol. 2, *Isothermal Laminar Flow*, 1020 pp., John Wiley, Hoboken, N. J.

Habashi, W., J. Dompierre, Y. Bourgault, D. Ait-Ali-Yahia, M. Fortin, and M. Vallet (2000), Anisotropic mesh adaptation: Towards user-independent, mesh-independent and solver-independent CFD. Part I: General principles, *Int. J. Numer. Methods Fluids*, *32*(6), 725–744.

Hecht, F. (2006), BAMG: Bidimensional Anisotropic Mesh Generator, technical report, FreeFem++, Paris.

Hutter, K. (1983), *Theoretical Glaciology: Material Science of Ice and the Mechanics of Glaciers and Ice Sheets*, 150 pp., D. Reidel, Dordrecht, Netherlands.

Joughin, I., S. Tulaczyk, J. Bamber, D. Blankenship, J. Holt, T. Scambos, and D. Vaughan (2009), Basal conditions for Pine Island and Twaites glaciers, West Antarctica, determined using satellite and airborne data, *J. Glaciol.*, *55*(190), 245–257.

MacAyeal, D. R. (1989), Large-scale ice flow over a viscous basal sediment: Theory and application to ice stream B, Antarctica, *J. Geophys. Res.*, *94*(B4), 4071–4087.

MacAyeal, D. (1993), A tutorial on the use of control methods in ice-sheet modeling, *J. Glaciol.*, *39*(131), 91–98.

Maule, C. F., M. E. Purucker, N. Olsen, and K. Mosegaard (2005), Heat flux anomalies in Antarctica revealed by satellite magnetic data, *Science*, *309*(5733), 464–467.

Nowicki, S. M. J., and D. J. Wingham (2008), Conditions for a steady ice sheet-ice shelf junction, *Earth Planet. Sci. Lett.*, *265*(1–2), 246–255.

Paterson, W. (1994), *The Physics of Glaciers*, 3rd ed., Pergamon, Oxford, U. K.

Pattyn, F. (2003), A new three-dimensional higher-order thermomechanical ice sheet model: Basic sensitivity, ice stream development, and ice flow across subglacial lakes, *J. Geophys. Res.*, *108*(B8), 2382, doi:10.1029/2002JB002329.

Rignot, E. (2008), Changes in West Antarctic ice stream dynamics observed with ALOS PALSAR data, *Geophys. Res. Lett.*, *35*, L12505, doi:10.1029/2008GL033365.

Rignot, E., D. Vaughan, M. Schmeltz, T. Dupont, and D. MacAyeal (2002), Acceleration of Pine Island and Thwaites glaciers, West Antarctica, *Ann. Glaciol.*, *34*, 189–194.

Thomas, R., E. Rignot, P. Kanagaratnam, W. Krabill, and G. Casassa (2004), Force-perturbation analysis of Pine Island Glacier, Antarctica, suggests cause for recent acceleration, *Ann. Glaciol.*, *39*, 133–138.

van den Broeke, M. (2008), Depth and density of the Antarctic firn layer, *Arct. Antarct. Alp. Res.*, *40*(2), 432–438.

van der Veen, C. J., and I. M. Whillans (1989), Force budget: I. Theory and numerical methods, *J. Glaciol.*, *35*, 53–60.

Vaughan, D. G., H. F. J. Corr, F. Ferraccioli, N. Frearson, A. O'Hare, D. Mach, J. W. Holt, D. D. Blankenship, D. L. Morse, and D. A. Young (2006), New boundary conditions for the West Antarctic ice sheet: Subglacial topography beneath Pine Island Glacier, *Geophys. Res. Lett.*, *33*, L09501, doi:10.1029/2005GL025588.

Vieli, A., and A. Payne (2003), Application of control methods for modelling the flow of Pine Island Glacier, West Antarctica, *Ann. Glaciol.*, *36*, 197–204.

Vogel, C. R. (2002), *Computational Methods for Inverse Problems*, Soc. for Ind. and Appl. Math., Philadelphia, Pa.

D. Aubry and H. Ben Dhia, Laboratoire MSSMat, UMR 8579, École Centrale Paris, CNRS, Grande Voie des Vignes, F-92295 Châtenay-Malabry CEDEX, France. (denis.aubry@ecp.fr; hachmi.ben-dhia@ecp.fr)

E. Larour, Thermal and Cryogenics Section, 354, Mechanical Division, Jet Propulsion Laboratory, California Institute of Technology, MS 157-316, 4800 Oak Grove Dr., Pasadena, CA 91109, USA. (eric.larour@jpl.nasa.gov)

M. Morlighem and H. Seroussi, Radar Science and Engineering Section, 334, Communication Tracking and Radar Division, Jet Propulsion Laboratory, California Institute of Technology, MS 300-319, 4800 Oak Grove Dr., Pasadena, CA 91109, USA. (mathieu.morlighem@jpl.nasa.gov; helene.seroussi@jpl.nasa.gov)

E. Rignot, Department of Earth System Science, University of California, Croul Hall, Irvine, CA 92697-3100, USA. (erignot@uci.edu)